Theoretical Equilibrium Shape of Calcite. 2. [$\bar{4}41$] Zone and Its Role in Biomineralization

ARTICLE *in* CRYSTAL GROWTH & DESIGN · AUGUST 2011

Impact Factor: 4.89 · DOI: 10.1021/cg2005584

4 AUTHORS:

Dino Aquilano
Università degli Studi di Torino
190 PUBLICATIONS **999** CITATIONS
SEE PROFILE

Marco Bruno
Università degli Studi di Torino
84 PUBLICATIONS **706** CITATIONS
SEE PROFILE

Francesco Roberto Massaro
University of Padova
41 PUBLICATIONS **286** CITATIONS
SEE PROFILE

Marco Rubbo
Università degli Studi di Torino
98 PUBLICATIONS **614** CITATIONS
SEE PROFILE

CRYSTAL GROWTH & DESIGN

ARTICLE

pubs.acs.org/crystal

Theoretical Equilibrium Shape of Calcite. 2. [$\bar{4}41$] Zone and Its Role in Biomineralization

Dino Aquilano,*[,†] Marco Bruno,[†] Francesco Roberto Massaro,[‡] and Marco Rubbo[†]

[†]Dipartimento di Scienze Mineralogiche e Petrologiche, Università degli Studi di Torino, Via Valperga Caluso 35, I-10125 Torino, Italy

[‡]Dipartimento di Scienza dei Materiali, Università degli Studi di Milano Bicocca, Via Roberto Cozzi 53, I-20125 Milano, Italy

ABSTRACT: The Hartman−Perdok analysis on the $\langle\bar{4}41\rangle$ zone of calcite was carried out, and the calculation of the surface and attachment athermal energies was performed on both unrelaxed and relaxed surfaces by using the interatomic Rohl potential and the GULP simulation code. The flat (F) character of the $\{10\bar{1}4\}$ and $\{11\bar{2}0\}$ forms and the stepped (S) character of the $\{01\bar{1}8\}$ and $\{21\bar{3}4\}$ forms contradict the observed occurrence frequency of natural crystals: $\{21\bar{3}4\} > \{01\bar{1}8\} > \{10\bar{1}4\} > \{11\bar{2}0\}$. A minor reduction of the relaxed surface energy values of both $\{01\bar{1}8\}$ and $\{21\bar{3}4\}$ forms could be sufficient to make the theoretical equilibrium shape of the crystal composed by the $\{10\bar{1}4\}$, $\{01\bar{1}2\}$, $\{10\bar{1}0\}$, $\{0001\}$, $\{01\bar{1}8\}$, and $\{21\bar{3}4\}$ forms, which can explain the richness of the growth morphology of calcite, even if water adsorption is not considered. The theoretical analysis is focused on the $\{21\bar{3}4\}$ scalenohedron to understand the adsorption of the enantiomers of some amino acids. Epitaxy models are described: (i) between the D and L $\{21\bar{3}4\}$ surfaces and the adsorbed 2D layers of polar $\{010\}$ and $\{0\bar{1}0\}$ L-Asp; (ii) between the $\{10\bar{1}4\}$ surfaces and the adsorbed 1D rows and 2D Asp layers; (iii) between the D and L $\{21\bar{3}4\}$ surfaces and the adsorbed 2D layers of the $\{011\}$ form of the alanine crystal. Hence, the enantiospecificity of the adsorption is better explained through a "cooperative molecular" approach, instead of searching for the best interaction of a single molecule on specific surface sites.

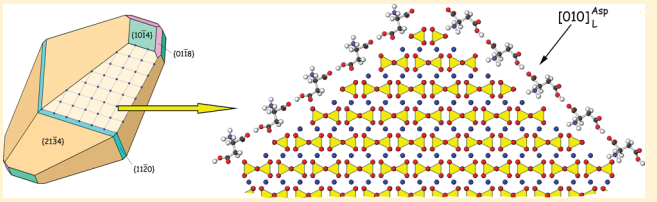

1. INTRODUCTION

The occurrence frequency of the $\{hk\bar{i}l\}$ forms of calcite, according to the observation on more than 2500 natural crystals,[1] disproves the widespread belief that the famous $\{10\bar{1}4\}$ cleavage rhombohedron is the most important one. Likely, this form could be dominant when calcite grows from pure aqueous solution at low temperature and supersaturation. However, natural crystals grown under variable conditions of temperature and supersaturation and, especially in the presence of inorganic and organic impurities, do not follow this rule, as can be seen in Table 1. Here, the Hartman−Perdok method,[2] which allows determination of the character of crystal faces, has been used. This method is based on the assumption that when a crystal grows, the growth units (atoms, ions, or molecules) coming from the mother phase enter the crystal, forming periodic chains of strong bonds in the first coordination sphere. Accordingly, these periodic bond chains (PBCs) form the true framework of the crystal structure and, consequently, of the growing faces. The classification of the character of the crystal faces, based on the PBC criterion, reads as follows: (i) Flat (F) faces are those where at least two families of PBCs run within a thickness d_{hkl} allowed by the systematic extinction rules. (ii) In the stepped (S) faces, only one family of parallel PBCs is found. (iii) In the kinked (K) faces, no PBCs can be found in the allowed d_{hkl} thickness.

Contrary to the usual conviction that only the F forms can belong to the growth shape of a crystal, the three main forms show a stepped character. Moreover, the principal $\{10\bar{1}0\}$ prism belongs as well to the athermal equilibrium shape of calcite, together with two F forms, $\{10\bar{1}4\}$ and $\{01\bar{1}2\}$, and a K form, $\{0001\}$, when the contribution of both surface reconstruction and relaxation on the surface energies of calcite is taken into account.[3] Four forms, out of eight, belong to the $[\bar{4}41]$ zone (Table 1). This is not due to chance since the $[\bar{4}41]$ direction corresponds to the most important PBC of calcite.[3,4] In this paper, we will compare the surface features of these four forms, taking advantage of the fact that we already investigated both the cleavage $\{10\bar{1}4\}$ rhombohedron and the secondary $\{11\bar{2}0\}$ prism.[3] Our interest is not confined to compare the behavior of the F faces with respect to the S ones and to understand why S forms such as $\{01\bar{1}8\}$ and $\{21\bar{3}4\}$ can become so morphologically relevant. Actually, it was demonstrated that the $\{21\bar{3}4\}$ scalenohedron adsorbs selectively L- and D-amino acids.[5−10] Thus, we want to determine the configurations of the surfaces belonging to the $[\bar{4}41]$ zone to find if the chiral molecule adsorption can occur either on the terraces or on the steps and if the adsorbate forms an unstructured layer of molecules rather than an epitaxial deposit.

2. CHARACTER, SURFACE STRUCTURE, AND ENERGIES OF THE FORMS BELONGING TO THE [$\bar{4}41$] ZONE

The projection of the calcite crystal along one out of the three equivalent $\langle\bar{4}41\rangle$ directions is illustrated in Figure 1. A $\langle\bar{4}41\rangle$ chain is built by an uninterrupted sequence, $\cdots Ca^{2+}-CO_3^{2-}-Ca^{2+}-CO_3^{2-}\cdots$, with a repeat period $^1/_3\langle\bar{4}41\rangle$ = 12.854 Å

Received: May 3, 2011
Revised: July 5, 2011
Published: July 18, 2011

dx.doi.org/10.1021/cg2005584 | *Cryst. Growth Des.* 2011, 11, 3985–3993

owing to the antiparallelism of two consecutive CO_3^{2-} groups. In this configuration, the electrical dipole moment perpendicular to the chain axis is canceled and then the chain is a true PBC in the sense of Hartman−Perdok (HP).[2] $Ca^{2+}-CO_3^{2-}$ bonds building up this PBC are the strongest ones which form during calcite crystallization, their labels and lengths (Å) being δ_1 = 2.360, δ_2 = 3.459, and δ_3 = 4.285. In Figure 1a we also draw the outermost unrelaxed slices of the forms belonging to the $\langle\bar{4}41\rangle$ zone; their thicknesses fulfill the conditions required by the systematic extinction rules (see Table 1).

2.1. {10$\bar{1}$4} and {11$\bar{2}$0} F Forms. Adjacent [$\bar{4}$41] PBCs are connected within the $d_{10\bar{1}4}$ and $d_{11\bar{2}0}$ slices. This is better pointed out in Figure 2, where the front views of the outermost layer of the {10$\bar{1}$4} and {11$\bar{2}$0} forms show the other PBCs running within the just mentioned slices.

2.1.1. {10$\bar{1}$4} Cleavage Rhombohedron. Concerning the (10$\bar{1}$4) face, the adjacent [$\bar{4}$41] PBCs are connected by the symmetry-equivalent [48$\bar{1}$] PBCs. These two families of principal PBCs form an angle ψ = 101.9° corresponding to the angle between the edges of the rhombohedron. Thus, the existence of two families of PBCs within this slice satisfies the condition necessary for the layer-by-layer growth of the {10$\bar{1}$4} form, which shows F character. Furthermore, this character is enhanced by the presence of two other kinds of PBCs within the slice: the [42$\bar{1}$] PBC, bisecting the angle ψ and the [010] PBC.[4] These secondary PBCs are not drawn in Figure 2 for the sake of clarity.

2.1.2. Secondary {11$\bar{2}$0} Prism. The faces of the {11$\bar{2}$0} prism are not as compact as the {10$\bar{1}$4} faces. As a matter of fact, the adjacent [$\bar{4}$41] PBCs are linked by the family of the [001] PBCs (represented in blue color in Figure 2). These PBCs are the weakest ones within the $d_{11\bar{2}0}$ slice, the $\cdots Ca^{2+}-CO_3^{2-}\cdots$ sequence being made in this case by δ_4 = 4.454 Å bonds. Also in this case one can find two other kinds of secondary PBCs within the outermost layer (not drawn in Figure 2): PBCs [2$\bar{2}$1] and [$\bar{1}$11], both being built by a linear combination of alternating segments $^1/_2$[001] and $^1/_6$[$\bar{4}$41]. Summing up, the {10$\bar{1}$4} and the {11$\bar{2}$0} forms can grow layer by layer, i.e., either by 2D nucleation or by spiral growth or by both these coexisting mechanisms competing in parallel.

2.2. {01$\bar{1}$8} and {21$\bar{3}$4} S Forms. A completely different situation appears when the stepped forms of the [$\bar{4}$41] zone are considered.

Table 1. Occurrence Frequency of the Main Crystallographic Forms of Natural Calcite Crystals Along with Their Character and the $d_{hk\bar{i}l}$ Equidistances Allowed by the Extinction Rules

form	thickness (Å) of the allowed slice	occurrence frequency (%)	character
{10$\bar{1}$0}	$d_{30.0}$ = 1.422	46.3	S
{21$\bar{3}$4}[a]	$d_{21.4}$ = 1.525	38.9	S
{01$\bar{1}$8}[a]	$d_{01.8}$ = 1.913	37.2	S
{10$\bar{1}$4}[a]	$d_{10.4}$ = 3.035	35.7	F
{01$\bar{1}$2}	$d_{01.2}$ = 3.860	24.2	F
{10$\bar{1}$1}	$d_{20.2}$ = 2.095	23.8	F
{0001}	$d_{00.6}$ = 2.845	17.2	K
{11$\bar{2}$0}[a]	$d_{11.0}$ = 2.495	14.1	F

[a] Belongs to the zone axis [$\bar{4}$41].

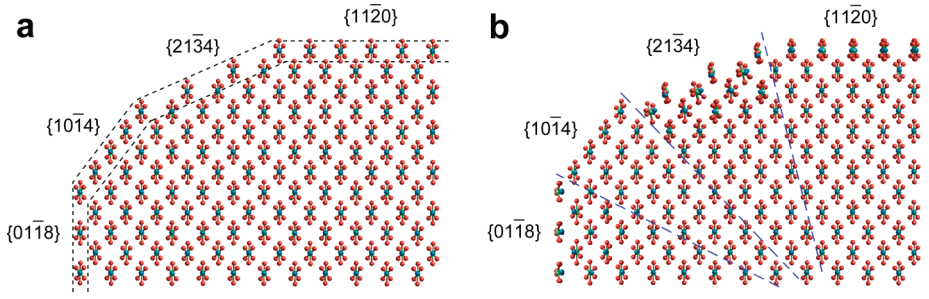

Figure 1. Calcite structure projected along the [$\bar{4}$41] zone axis: calcium atoms (blue), carbonate groups (red); unrelaxed (a) and relaxed (b) surface profiles of the main forms belonging to the zone. Dashed lines represent the slice thickness allowed by the extinction rules (a) and separate the growth sectors of the different forms (b).

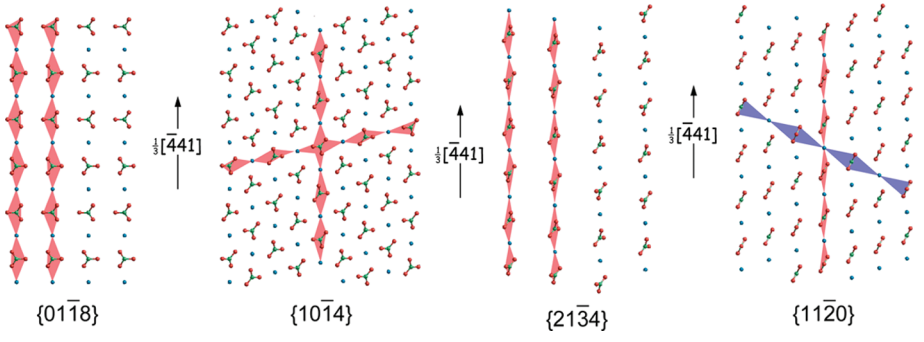

Figure 2. Front view of the outermost layer of the forms belonging to the [$\bar{4}$41] zone. Their character comes out from the bonds between the [$\bar{4}$41] PBCs. {01$\bar{1}$8}, the "flat" rhombohedron, and {21$\bar{3}$4}, the scalenohedron, do not show bonds between adjacent [$\bar{4}$41] PBCs and hence are S forms. {10$\bar{1}$4}, the cleavage rhombohedron, and the prism {11$\bar{2}$0} show F character since the [$\bar{4}$41] PBCs are bonded by the symmetry-equivalent [48$\bar{1}$] PBCs and by the [001] PBCs, respectively.

dx.doi.org/10.1021/cg2005584 |*Cryst. Growth Des.* 2011, 11, 3985–3993

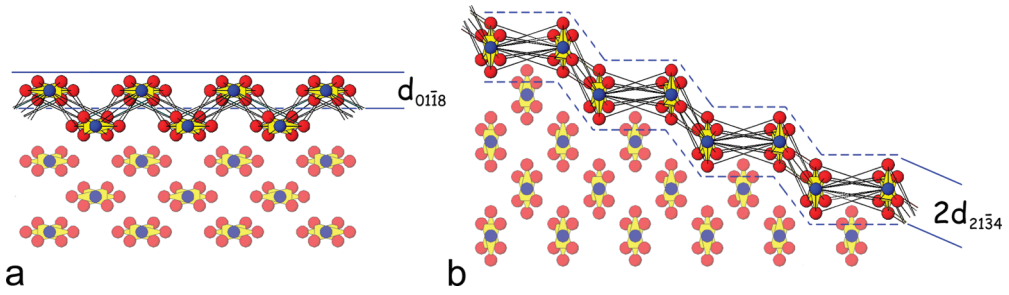

Figure 3. Detailed surface profiles of the stepped faces: (a) $(01\bar{1}8)$ and (b) $(21\bar{3}4)$ viewed along the $[\bar{4}41]$ PBC. Within the $d_{01\bar{1}8}$ slice, no bond develops between adjacent PBCs while strong δ_1, δ_2, and δ_3 bonds link contiguous PBCs, giving rise to a wavy surface within a $2d_{01\bar{1}8}$ slice. An analogous result obtains within a $2d_{21\bar{3}4}$ slice where the alternating segments are built by δ_1, δ_2, and δ_3 bonds and δ_4 bonds.

2.2.1. $\{01\bar{1}8\}$ Stepped Rhombohedron. According to Figure 3a, no bonds between neighboring $[\bar{4}41]$ PBCs can be found within a slice of thickness $d_{01\bar{1}8}$. Moreover, from Figure 2, it is clear that the repulsion among $[\bar{4}41]$ chains in the slice can reach a relative maximum owing to the facing of ions of the same sign. Thus, the instability of $[\bar{4}41]$ monolayered steps is not surprising, as we proved when estimating the athermal unrelaxed edge energy $\rho_{\bar{4}41}^{\text{monolayer}} = -3.515 \times 10^{-5}$ erg cm^{-1}.[11] As a consequence, this form cannot grow by layers of elementary $d_{01\bar{1}8}$ thickness since there is one step (on the face) showing a negative edge energy.

Nevertheless, a layer twice as thick has a positive $[\bar{4}41]$ edge energy on the $(01\bar{1}8)$ face owing to the strong δ_1, δ_2, and δ_3 bonds linking the PBCs within a $2d_{01\bar{1}8}$ slice (see Figure 3a). As a matter of fact, we calculated $\rho_{\bar{4}41}^{\text{bilayer}} = +2.46 \times 10^{-5}$ erg cm^{-1}.[11]

In turn, the question to be answered is how bilayers (or multiple layers) can originate on the $(01\bar{1}8)$ face.

(i) One way is to consider that $[\bar{4}41]$ chains can form at supersaturation, independently of each other, onto the $\{01\bar{1}8\}$ surfaces, giving rise to a *fluctuating wavy surface made by strongly elongated microfacets that expose their stable $\{10\bar{1}4\}$ profile* toward the mother phase.[11] This growth model does not change the character of the $\{01\bar{1}8\}$ form from stepped to flat; nevertheless, as much as the $\{10\bar{1}4\}$ microfacets increase their extension and coverage on the $\{01\bar{1}8\}$ surfaces, the diffusion processes transforms from 1D (along the steps) to 2D (on the microfacets). Hence, the role exerted by the surface diffusion can be enhanced and the average normal growth rate of the face should be lowered and its morphological importance increased at the expense of the adjacent forms as occurs in natural crystals.

(ii) A second mechanism is related to the role played by dislocations. The slip system in calcite develops in the planes $10\bar{1}4$, $01\bar{1}8$, and $01\bar{1}2$, and the minimum length of the Burgers vectors is $^1/_3\langle 42\bar{1}\rangle$ = 8.103 Å.[12] Then it is sufficient that either an edge or a screw dislocation outcrops on a free $\{01\bar{1}8\}$ surface with the normal component of its Burgers vector larger than $2d_{01\bar{1}8}$ = 3.826 Å for a stable $[\bar{4}41]$ double edge form and spreads (or winds, originating a growth spiral) on the surface.

2.2.2. $\{21\bar{3}4\}$ Stepped Scalenohedron. According to Figure 3b, no bonds between adjacent $[\bar{4}41]$ PBCs can be found within a slice of thickness $d_{21\bar{3}4}$. Hence, also the $\{21\bar{3}4\}$ form cannot grow by lateral spreading of $d_{21\bar{3}4}$ monolayers. To find a correlated growth between adjacent $[\bar{4}41]$ chains, one has to consider slices of thickness equal to $2d_{21\bar{3}4}$: in this case the resulting surface profile of the face can be imagined as composed by alternating segments of $(10\bar{1}4)$ and $\{11\bar{2}0\}$ microfacets whose lengths are 3.15 and 3.82 Å, respectively. Figure 3b indicates the δ_1, δ_2, and δ_3 bonds linking the $[\bar{4}41]$ chains within the $(10\bar{1}4)$ segments, while the $(11\bar{2}0)$ microfacets are built by the weaker δ_4 bonds.

Mutatis mutandis, by the same arguments invoked in the case of the $\{01\bar{1}8\}$ faces, multiple $d_{21\bar{3}4}$ layers can form and slow the growth rate of these faces.

2.3. Calculation Method of Specific Surface (γ) and Attachment (E_{att}) Energies. Calculations (optimizations of slab geometries and surface and attachment energies) were performed by using the interatomic potential for calcite developed by Rohl et al.[13] (Rohl potential hereinafter) and the General Utility Lattice Program (GULP) simulation code,[14] which, being based on force field methods, allows the calculation of the structures and properties of minerals from a given set of empirical potentials. Geometry optimization is considered converged when the gradient and the function tolerance (*gtol* and *ftol* adimensional parameters in GULP) are smaller than 0.0001 and 0.00001, respectively.

The surfaces were studied by using the 2D slab model.[15] The slabs of varying thickness were generated by separating the bulk structure along the plane of interest. The calculations were performed by considering the original (1×1) cells.

The geometry optimization was performed by means of the Newton−Raphson method and by considering the slab subdivided into two regions: region 1, which contains both the surface and the underlying atomic layers that are allowed to relax, and region 2, which has the same number of layers as region 1 and contains the rest of the slab material where no relaxation with respect to the bulk crystal structure is assumed to occur.

Calculations were done by considering slabs with thicknesses up to 10 layers (in both regions 1 and 2), which are sufficient to reproduce bulklike properties at the center of the slab and to obtain a careful description of the surface. According to the standard two-region strategy employed by GULP, the specific surface energy (γ, erg cm^{-2}) was evaluated from the energy of the surface block (U_s, region 1) and the energy of a portion of the bulk crystal (U_b) containing the same number of atoms as the surface block. Both energies have been referred to A, the common surface area of the primitive unit cell:

$$\gamma = \frac{U_s - U_b}{A} \tag{1}$$

A 10-layer slab (in both regions 1 and 2) was sufficient to reach convergence on the γ values. The attachment energy, $E_{\text{att}}^{hk\bar{i}l}$

dx.doi.org/10.1021/cg2005584 |*Cryst. Growth Des.* 2011, 11, 3985–3993

Table 2. Surface (Relaxed and Unrelaxed) and Attachment (Unrelaxed) Energies in the $[\bar{4}41]$ Zone[a]

form	$\{10\bar{1}4\}$-F	$\{11\bar{2}0\}$-F	$\{01\bar{1}8\}$-S	$\{21\bar{3}4\}$-S
thickness (Å) of the allowed slice	3.035	2.495	1.913	1.525
equidistance (Å) between the $[\bar{4}41]$ PBCs	3.150	3.825	4.990	6.256
interaction energy (erg mol^{-1}) $\times$ 10^{12} between $[\bar{4}41]$ PBCs within the allowed d_{hkl} layer	−2.807	0.825	0.598	0.046
$\gamma_{unrelaxed}$ (erg cm^{-2})	707	1812	1253	1451
$\gamma_{relaxed}$ (erg cm^{-2})	536	1232	702	783
$\Delta\gamma$ (%) = $(\gamma_r - \gamma_u)/\gamma_u$	−24.18	−32.01	−43.97	−46.04
$E_{attachment}$ (10^{-12} erg molecule^{-1})	2.969	9.722		

[a] The reduction, $\Delta\gamma$ (%), due to the surface relaxation is also indicated. $E_{attachment}$ values of the $\{01\bar{1}8\}$ and $\{21\bar{3}4\}$ forms were not calculated since the attachment energy of stepped forms is meaningless.

(the energy released, per growth unit, when a stoichiometric layer of material is added onto the surface), is given by

$$E_{att}^{hk\bar{i}l} = U_{tot}^{n+1} - U_{tot}^{n} - U_{tot}^{1} \quad (2)$$

where U_{tot}^{n} represents the total internal energy of a surface model consisting of n growth layers and U_{tot}^{1} is the energy of the growth layer alone. In practice, the calculation of this exothermic quantity is obtained from the interaction energy of the growth layer at the surface with the rest of the underlying material.

2.4. Specific Surface (γ) and Attachment (E_{att}) Energy Values. The $\{10\bar{1}4\}$ rhombohedron shows the lowest value of the specific surface energy among all the calcite forms. This is hardly unexpected if one takes into account that four out of the strongest PBCs of the crystal develop within a $d_{10\bar{1}4}$ layer while only one $[\bar{4}41]$ PBC crosses the successive adjacent $10\bar{1}4$ layers. A further criterion confirming this rhombohedron property comes from Bravais−Friedel[16] and Donnay−Harker[17] (BFDH), who correlated the occurrence frequency of an $\{hkl\}$ form with its interplanar spacing d_{hkl}, the importance of the form increasing with the d_{hkl} value allowed by the systematic extinction rules: in our case, the highest layer thickness (3.035 Å) is that of the $\{10\bar{1}4\}$ form. Finally, the equidistance of 3.150 Å between adjacent $[\bar{4}41]$ PBCs within the $d_{10\bar{1}4}$ slice is by far the shortest one among all the forms belonging to the $[\bar{4}41]$ zone.

On the contrary, both BFDH and HP rules fail in foreseeing the stability of the other forms of this zone. In fact, both the sequence of thickness of the allowed slices (Table 2) and the character of the forms are not coherent with their observed morphological importance (Table 1). This discrepancy is sharply emphasized when comparing the $\gamma_{11\bar{2}0}$ value with those of the stepped $\{01\bar{1}8\}$ and $\{21\bar{3}4\}$ forms. We observe that the surface energies of the unrelaxed stepped forms, $\{01\bar{1}8\}$ and $\{21\bar{3}4\}$, are respectively −30.85% and −19.92% lower than that of the F form $\{11\bar{2}0\}$. The reduction is further enhanced (−43.02% and −36.44%, respectively) when relaxation is considered.

This proves, once again,[3] that the list of faces belonging to the equilibrium shape (ES) of an ionic crystal does not necessarily show *all* the F forms in the first place: forms classified as S can be more stable than F faces, especially when strong anisotropy factors intervene in the crystal structure, such as the shape of the carbonate ion in calcite.

Two more considerations can be drawn from the analysis of the relaxed γ values. The athermal values of 702 and 783 erg cm^{-2}, shown in Table 2, are so low that both the $\{01\bar{1}8\}$-S and $\{21\bar{3}4\}$-S forms can compete with the $\{10\bar{1}4\}$-F, $\{10\bar{1}0\}$-S, $\{01\bar{1}2\}$-F, and $\{0001\}$-K forms belonging to the athermal ES of the calcite crystal.[3] As a matter of fact, some factors reducing both $\gamma_{01\bar{1}8}$ and $\gamma_{21\bar{3}4}$ by less than 3% cause the $\{01\bar{1}8\}$ and $\{21\bar{3}4\}$ forms to appear on the ES. This should be easily achieved by a temperature increase, having considered that the vibrational and configurational contributions ($-TS$) to the surface energy ($\gamma = \gamma_{0K} - TS$) are by far larger for stepped faces than for the flat ones. The low value of $\gamma_{01\bar{1}8}$ for both relaxed and unrelaxed surfaces allows one to account for the $01\bar{1}8$ cleavage system of calcite, commonly observed as ready parting along twin lamellae on $\{01\bar{1}8\}$.[12] Thus, we are able, for the first time, to explain this secondary cleavage system by coupling the low $\gamma_{01\bar{1}8}$ value with the easy gliding along the $[\bar{4}41]$ direction, as ensues from literature data and from the wavy surface described in Figure 3a.

3. EPITAXIAL BEHAVIOR OF THE $\{21\bar{3}4\}$ SCALENOHEDRON AND $\{10\bar{1}4\}$ CLEAVAGE RHOMBOHEDRON: ADSORPTION AND ENANTIOSPECIFICITY

As mentioned above and illustrated in Figures 2 and 3, the $\langle\bar{4}41\rangle$ PBC is the only one structuring the faces of the $\{21\bar{3}4\}$ form. Notwithstanding this, one can find on the $\{21\bar{3}4\}$ surfaces a 2D cell (Figures 4 and 5) defined by a second relevant direction. We choose the following parameters:

(i) $^1/_3\langle\bar{4}41\rangle$ = 12.850 Å, which is parallel to the intersections between the faces of indices $(21\bar{3}4)$ and the equivalent ones $(12\bar{3}\bar{4})$ related by the A_2 axes. The repeat period of Ca^+ or CO_3^{2-} ions along this direction is half the PBC period, i.e., $^1/_6[\bar{4}41]$ = 6.425 Å.

(ii) $^1/_3\langle12\bar{1}\rangle$ = 6.375 Å, parallel to the intersections between the faces of indices $(21\bar{3}4)$ and the equivalent ones $(\bar{2}3\bar{1}4)$ related by the mirror planes. In this case the repeat period coincides with the vector $^1/_3\langle12\bar{1}\rangle$.

Furthermore, the angle ε between the vectors $^1/_3\langle\bar{4}41\rangle$ and $^1/_3\langle12\bar{1}\rangle$ is 101.08°.

Downs et al.[7] make a different choice of the surface 2D cell on the same scalenohedron (Figure 5) characterized by the parameters $a = {}^1/_3\langle\bar{1}20\rangle$ = 13.202 Å, $b = {}^1/_3\langle12\bar{1}\rangle$ = 6.375 Å, and γ = 107.21°, where γ represents the angle between the vectors $^1/_3\langle\bar{1}20\rangle$ and $^1/_3\langle12\bar{1}\rangle$. This is a correct choice, of course, but is not sensible from the morphological point of view. As a matter of fact, this cell does not completely account for the growth morphology of the crystal since the direction $\langle\bar{1}20\rangle$ is not related to any important structural feature of the scalenohedron. According to Haüy, by "important features" we mean either the edges (both existing and theoretically possible) between the faces or the steps limiting 2D nuclei and/or spirals from spreading onto

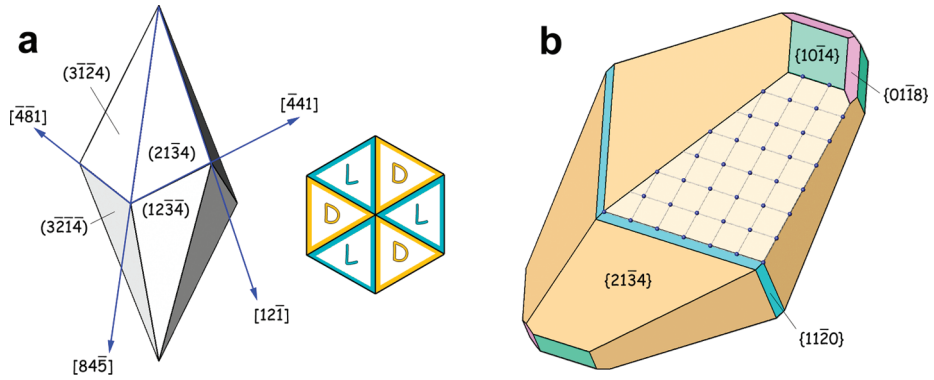

Figure 4. (a) {21$\bar{3}$4} form of calcite with the directions of the edges between the equivalent faces. The up−down view along the [001] direction schematically represents the faces (D, L) related by the symmetry planes according to Hazen's labeling. (b) All the forms belonging to the zone ⟨$\bar{4}$41⟩ axis are represented, with the prevailing scalenohedron, for the sake of clarity. On the (21$\bar{3}$4) face of the scalenohedron, the repeat periods of Ca ions lying in the outermost $d_{21\bar{3}4}$ layer are also represented.

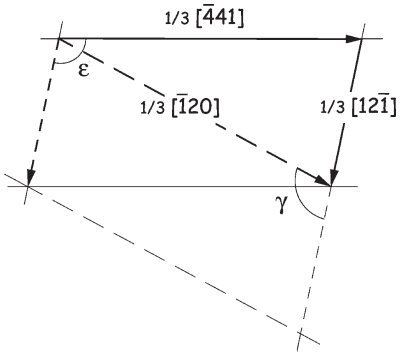

Figure 5. Elementary 2D cells that can be drawn on the (21$\bar{3}$4) face of the calcite scalenohedron. Our choice is represented by full vectors, while dashed vectors refer to the Downs et al.[7] cell. Vectors $^1/_3$[$\bar{4}$41] and $^1/_3$[12$\bar{1}$] can also be found in Figure 4a.

the surfaces; these develop as sequences of the strongest PBCs of the crystal according to the Hartman way of thinking.

Our choice fulfills the requirement of the cell as an important feature since the ⟨12$\bar{1}$⟩ direction is parallel to the intersections between the faces (D, L) of the scalenohedron [here we used, according to Hazen, the labels D and L to indicate a couple of scalenohedron faces related by a mirror plane (see Figure 4a); nevertheless, these labels, which are useful and correct for molecular enantiomers, seem to be ambiguous when applied to symmetry-equivalent faces], while the ⟨$\bar{4}$41⟩ direction not only coincides with the strongest PBC of the crystal but is also parallel to the intersections between the rhombohedron faces which are related by the diad axes. Moreover, as we will show later on, the ε angle of 101.08° assumes, at variance with the angle γ =107.21°, a strategic role in the selective adsorption of chiral molecules on the scalenohedron surfaces.

Hazen et al.[10] experimentally showed negligible enantiospecificity for alanine on the calcite scalenohedron and examined the adsorption of both Ala enantiomers on the (21$\bar{3}$4) surface by performing ab initio calculations at the DFT level. They found very small differences in the binding energy and structure for the global minimum of the D- and L-Ala on the mentioned surfaces and ascribed the weak enantiospecificity to the size disparity between the Ala molecules and the distances between atoms lying on the surfaces of the calcite scalenohedron.

Furthermore, they experimentally found that L-Asp adsorbs *preferentially* versus D-Asp on the L-faces of the scalenohedron (see Figure 4a), while the inverse was found on the D-faces of the same form.[5,8] From the combination of all these results, the importance of the size of the adsorbed amino acid and that "...the larger amino acid, such as Aspartic, may show stronger enantiospecificity...".[10] are clear.

For the time being, we will not discuss these conclusions, but we outline that the interpretation proposed on the enantioselective adsorption is grounded on the interaction of a single molecule of the adsorbate with the crystalline substrate and the structure of the substrate is not viewed as a set of well-ordered bond chains, which is physically sensible but as a distribution of different atomic species at different levels with respect to the average crystallographic plane.

Our way of thinking starts from the experience we gained in experimental and theoretical investigations on the adsorption/absorption phenomena occurring in calcium and barium carbonates growing from aqueous solutions in the presence of specific additives.[11,16,18−22] Accordingly, we were induced to extend the model of 2D epitaxial adsorption to the interpretation of the enantioselectivity of the two couples {21$\bar{3}$4} calcite/aspartic acid and {21$\bar{3}$4} calcite/alanine.

3.1. 2D Epitaxial Model: {21$\bar{3}$4} Calcite/{010} Aspartic Acid. Let us recollect the cell parameters of L-aspartic acid, a_0 = 7.61, b_0 = 6.982, c_0 = 5.142 Å, β = 99.84°, and consider the d_{020} slice, which is allowed by the systematic extinction rules.[23] Owing to the $P2_1$ space group, this slice contains one molecule per unit cell and does show polarity along the *y*-axis due to the lack of mirror symmetry (i.e., the 010 plane). Let us superimpose now the d_{020} Asp slice onto the (21$\bar{3}$4) D-face of calcite and turn it around its *y*-axis until the $[100]_{Asp}$ and $[001]_{Asp}$ vectors coincide with the scalenohedron edges [$\bar{4}$41] and [12$\bar{1}$], respectively. The coincidence lattice occurring at the resulting calcite/Asp interface is illustrated in Table 3.

Since an excellent fit between the lattice geometry of calcite and that of Asp ensues from Table 3, we were induced to hypothesize a 2D epitaxy between a d_{020} slice of Asp and a (21$\bar{3}$4) face of the calcite scalenohedron.

To do this, one has to verify that two conditions are fulfilled so that a 2D epitaxy can set in.

The *first one* concerns the mother phase. As a matter of fact, a 2D epitaxy can be obtained if the mother solution is unsaturated

Table 3. Coincidence Lattice and Angular Misfit between the $(21\bar{3}4)$ D-Face of Calcite and the (010) Face of Aspartic Acid

vector (Å) of the 2D coincidence cell on the $(21\bar{3}4)$ D-face of calcite	vector (Å) of the 2D coincidence cell on the (010) face of aspartic acid	misfit (%)
$3 \times {}^1/_3[\bar{4}41] = 38.549$	$5 \times [100] = 38.085$	+1.22
$4 \times {}^1/_3[12\bar{1}] = 25.499$	$5 \times [001] = 25.71$	−0.83
ε = angle between $[\bar{4}41]$ and $[12\bar{1}] = 101.08°$	γ = angle between [100] and [001] = 99.84°	angular misfit +1.24°
area of the 2D coincidence cell 964.64 Å^2	area of the 2D coincidence cell 964.76 Å^2	−0.0012

with respect to the acid; otherwise, if the solution is supersaturated with respect to the acid, a 3D epitaxy can occur on the substrate.[24] In the experiments carried out by Hazen et al.,[5,25,26] the solutions used for the adsorption measurements were largely unsaturated with respect to the Asp's. Hence, the first condition is fulfilled.

The *second one* concerns the adhesion energy of the adsorbed molecule. For a 2D epitaxy to occur, the "vertical bonds" between the adsorbed molecule and the substrate must be stronger than the "lateral bonds" formed among molecules within the adsorbed layer.[24]

Experiments proved that both racemic[25,26] and D/L[5] Asp are strongly adsorbed onto the calcite scalenohedron. Moreover, the calculations show that the d_{020} Asp layers can be adsorbed[7,9] thanks to the three strong points of interaction (two Ca atoms from the calcite bond to O atoms of the two carboxyl groups of Asp, and O atoms from the carbonate groups of calcite bond to the amino group from Asp) when D-Asp bonds to the $(21\bar{3}4)$ D-face of the calcite scalenohedron and the two strong points of interaction formed by L-Asp with the same surface.

One can summarize that the second condition for the formation of a 2D epitaxy is largely fulfilled since it is reasonable to assume that the "vertical bonds" calcite−Asp are stronger that the OH−O and NH−O "lateral bonds" formed among Asp molecules within the d_{020} adsorbed layer.[23]

3.1.1. Enantiospecificity of the d_{020} Epitaxially Adsorbed Layers of Aspartic Acid onto the Calcite Scalenohedron. The existence of epitaxial monolayers of Asp of thickness $d_{020} = 3.491$ Å implies a well-defined orientation of the Asp molecules (or the zwitterions) with respect to the scalenohedron substrate. In other words, the adsorbed monolayer must behave as a polar one; i.e., the (010) face of the monolayer is the complementary one of its opposite $(0\bar{1}0)$ (Figure 6). Moreover, the (010) face of the crystalline L-Asp is the mirror image of the $(0\bar{1}0)$ face of D-Asp. This means that the enantioselectivity does not depend on the surface structure of the $(21\bar{3}4)$ and $(\bar{2}3\bar{1}4)$ faces of the scalenohedron (which are exactly the same, being symmetrically equivalent), but on the coupling between the substrate and the properly oriented epitaxial layer of molecules of suitable chirality.

To emphasize this concept, let us recollect the findings of Hazen et al.,[5,10] who pointed out that "...L-aspartic acid adsorbs *preferentially* on the L-faces of the scalenohedron, whilst the inverse was found on the D-faces of the same form...". If this is true, and there is no reason to question this statement, then the L-Asp molecules adsorbing onto the L-faces of the scalenohedron must adhere to the calcite face with the (010) side of their d_{020} monolayer. The complementary situation can set up on the D-faces of the scalenohedron where the epitaxial interaction will be fulfilled (both geometrically and structurally) only if the d_{020} monolayer of D-Asp will expose to the calcite face its $(0\bar{1}0)$ side.

The formation of epitaxially adsorbed 2D layers of foreign substances onto crystalline substrates is widely documented.

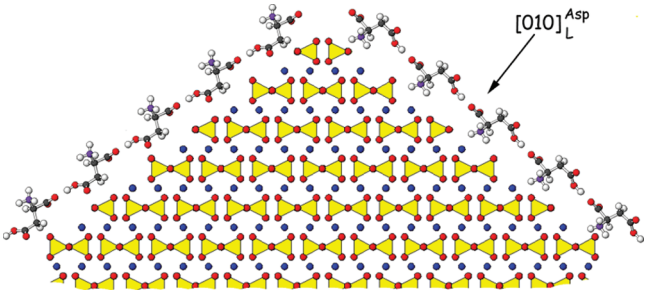

Figure 6. Calcite structure projected along the $[12\bar{1}]$ direction, which is the common edge of the $(21\bar{3}4)$ and $(\bar{2}3\bar{1}4)$ faces of the scalenohedron (blue atoms, Ca; yellow triangle and red atoms, carbonate groups). Two d_{020} monolayers of L-aspartic acid, viewed along their common [001] direction, are epitaxially superimposed onto scalenohedron faces. On the right side the interface is (010) L-Asp/$(\bar{2}3\bar{1}4)$ calcite, where the amino groups bond the O atoms of the carbonate ions. On the left side, where the interface is $(0\bar{1}0)$ L-Asp/$(21\bar{3}4)$ calcite, the complementary bonds form. This shows that the L-Asp enantiomorph adsorbs *preferentially* on one face. If (010) L-Asp/$(\bar{2}3\bar{1}4)$ is the optimal epitaxial layer, then its mirror image, D-Asp, should fit on $(21\bar{3}4)$.

In the case of solution growth, this occurs when the crystal does not form, as a rule, a solid solution with the foreign substance which is dissolved at the level of impurity. However, the impurity can adsorb on several faces, modifying the equilibrium and growth morphology of the crystal. In the present discussion, the interesting case is the global equilibrium among the crystal, the adsorbed layer, and the solution, obviously unsaturated in the impurity. In particular, the adsorbed layer can be unstructured or can show patches of equally oriented 2D epitaxial layers. As shown in the previous section, there are conditions making the epitaxy possible. Thus, the good interaction of an isolated molecule with the crystal surface is a necessary condition, but the very essential phenomenon is the tendency to form an ordered layer of compatible chiral molecules that adapts itself to the substrate structure. Consequently, it would be better to change our mind on the cause of the enantioselectivity. A further useful example, alanine adsorption on the calcite scalenohedron, will be described in section 3.3.

3.2. 2D Epitaxial Model: $\{10\bar{1}4\}$ Calcite/{010} Aspartic Acid. According to Hazen et al.,[5] the cleavage $\{10\bar{1}4\}$ rhombohedron of calcite strongly adsorbs from solution the racemic Asp. This rhombohedron has been used as an experimental control since its surface structure (crossed by a perpendicular symmetry glide plane) should not selectively adsorb L- or D-amino acids.

In fact, it is not by chance that that the mean D/L ratio of 0.9964 measured on the $\{10\bar{1}4\}$ form, which adsorbed Asp, was proved to be consistent with the 0.9948 ± 0.0015 D/L value observed for the Asp experimental solution.[5]

Also in this case we attempted to interpret this strong adsorption in light of the 2D epitaxy and found the results illustrated in Table 4.

Table 4. Coincidence Lattice and Angular Misfit between the $\{10\bar{1}4\}$ Form of Calcite and the (010) Face of Aspartic Acid

vector (Å) of the 2D coincidence cell on the $(10\bar{1}4)$ face of calcite	vector (Å) of the 2D coincidence cell on the (010) face of aspartic acid	misfit (%)
$3 \times {}^1/_3[\bar{4}41] = 38.549$	$5\times [100] = 38.085$	+1.22
$2 \times {}^1/_3[\bar{4}81] = 25.708$	$5\times [001] = 25.710$	−0.0006
$\chi = 101.85°$ (angle between $[\bar{4}41]$ and $[\bar{4}81]$)	$\gamma = 99.84°$ (angle between [100] and [001])	angular misfit +2.007°
area of the (3×2) coincidence cell on the $(10\bar{1}4)$ face of calcite 970.339 Å^2	area of the 2D (5×5) coincidence cell on the (010) face of Aspartic acid 964.76 Å^2	+0.058

Surprisingly, (010) Asp/$\{10\bar{1}4\}$ calcite and (010) Asp/$(21\bar{3}4)$ calcite epitaxies are more or less equivalent from the geometrical point of view: the parametric fit is even better on the rhombohedron, while the angular misfit is lower on the scalenohedron, and the areas of the 2D coincidence cells are practically the same in both cases. This means that both experimental data and geometrical fits play in favor of the existence (at equilibrium) of an adsorbed d_{020} monolayer facing the rhombohedron either with the (010) surface of L-Asp or with the $(0\bar{1}0)$ surface of D-Asp. It is also clear that both surfaces should fit, with the same adhesion energy, on the rhombohedron.

The lattice coincidences detailed in Table 4 make evident another important feature of the epitaxial adsorption of Asp. In fact, the vectors $2 \times {}^1/_3[\bar{4}81]_{calcite}$ and the vector $5 \times [001]_{aspartic}$ realize a quasi-perfect matching over a period close to 26 Å, while only an excellent fit obtains between the vectors $3 \times {}^1/_3[\bar{4}41]_{calcite}$ and the vector $5 \times [100]_{aspartic}$ over a larger period, close to 38 Å. This discrepancy assumes a relevant role if one remembers that the directions $\langle\bar{4}41\rangle$ and $\langle\bar{4}81\rangle$ are symmetry equivalent (owing to the $\langle 1\bar{2}10\rangle$ glide mirrors) and model the shape of 2D nuclei and/or of the spiral spreading onto the rhombohedron faces growing from pure aqueous solutions.[27]

As experimentally shown by Teng et al.,[28] the shape of spiral hillocks become asymmetric when Asp is added to the solution: new step directions appear, terrace widths change, and step corners become highly rounded. A qualitative interpretation was proposed by assigning these changes partially to kinetic factors and partially to the alteration of the equilibrium thermodynamic of the growth surface. Going into detail, the reduced terrace widths were attributed to a reduction of the step edge energy (smaller than for a step obtained from pure calcite solution by a factor of about 3). This was reasonably explained through the formation of *"...an ordered adsorption layer on the facets defined by the new step directions..."*.

Now, we can prove that this intuition was right as a whole and that the *ordered adsorption layer on the facets* is nothing more than a 1D epitaxy between Asp molecular arrays and growing calcite steps. Two factors are to be considered to explain the complexity of the adsorption phenomena ruling the equilibrium shape of 2D nuclei (and hence of the growth spirals) on the rhombohedron face:

(i) First, the mirror symmetry is broken when Asp molecules adsorb on the steps, owing to the asymmetry introduced by the different 1D epitaxies along the $\langle\bar{4}41\rangle$ and $\langle\bar{4}81\rangle$ step edges (see Table 4).

(ii) Second, one has to remember that the couple of steps $[\bar{4}41]_{acute}$ and $[\bar{4}81]_{acute}$ and the complementary one, made by the steps $[\bar{4}41]_{obtuse}$ and $[\bar{4}81]_{obtuse}$, form an acute and the complementary obtuse angle with the terrace substrate, respectively. Moreover, it has been demonstrated[29−31] that while the edge free energy of the unrelaxed steps (either acute or obtuse) should be the same, the steps undergo different relaxations (and then will show different free energies) according to whether they form an acute or an obtuse dihedral angle with the same substrate. In turn, this implies different adhesion energies between the relaxed steps and the 1D epitaxially adsorbed Asp molecular arrays.

When summarizing, the details of the 2D epitaxial model $\{10\bar{1}4\}$ calcite/{010} aspartic acid allow one to explain the lack of any symmetry in the growth (dissolution) patterns of the calcite rhombohedron when aspartic acid is added to the mother phase. 2D epitaxy affects the terraces between the growing steps, while 1D epitaxy changes the equilibrium shape of the 2D nuclei through a differential reduction of the free energy of the step edges (determining the nucleus shape and, consequently, the equidistances between spiral steps in the different growth sectors).

Finally, one has to take into account the following:

(i) The Asp adsorption should cooperate, with water as a solvent, in the lowering of the edge free energy of the steps running onto the rhombohedron.

(ii) The unrelaxed structure of the edges $\langle\bar{4}41\rangle$ and $\langle\bar{4}81\rangle$ (either acute or obtuse) is nothing other than $\{10\bar{1}4\}$ terraces, and then the *upper limit* of their free energy $\rho^{10\bar{1}4}_{[\bar{4}41]}$ (in aqueous solution at room temperature) should correspond to a consolidated experimental surface free energy ($\gamma_{10\bar{1}4}$) value of about 100 erg cm^{-2}.[4] Recollecting that $\rho^{10\bar{1}4}_{[\bar{4}41]} = \gamma_{10\bar{1}4}d_{10\bar{1}4}$, it turns out to be $\rho^{10\bar{1}4}_{[\bar{4}41]} \leq 100$ erg cm^{-2} $\times$ 3.03×10^{-8} cm $= 3.03 \times 10^{-6}$ erg cm^{-1}.

These considerations point out that the $\rho^{10\bar{1}4}_{[\bar{4}41]}$ values, ranging between 3.44×10^{-5} and 3.40×10^{-5} erg cm^{-1} and calculated by Teng et al. from their experimental kinetic data,[28] should be handled with care.

3.3. Nonenantiospecificity of the d_{011} Epitaxially Adsorbed Layers of Alanine onto the Calcite Scalenohedron. Let us now consider the geometry of the epitaxial relationship we found between a d_{011} layer of the L-alanine crystal ($a_0 = 5.940$, $b_0 = 12.274$, $c_0 = 5.806$ Å, space group $P2_12_12_1$)[31] and the $(21\bar{3}4)$ face of the calcite scalenohedron acting as a substrate (Table 5). This represents an example of an excellent coincidence lattice that can set up at the interface between the calcite scalenohedron and an alanine monolayer.

Then one can say that to suppose the existence of adsorbed epitaxial d_{011} slices of alanine on the calcite scalenohedron is consistent with both the experimental[10] and theoretical data (Figure 7).

However, it is worth remembering here that the molecular content of the d_{011} slices is symmetry related by a 2_1 axis which lies in the middle of the slice. Thus, surface profiles of the (011) and $(0\bar{1}1)$ faces are equivalent, contrary to what happens with the polarity shown by the d_{020} monolayer of Asp (where the 2_1 axis is perpendicular to the layer).

This implies that on the 2D cell of the $(0\bar{1}1)$ and (011) surfaces the same groups outcrop. These are, in the case of L-Ala,

Table 5. Lattice Coincidences and Angular Misfit between the $(21\bar{3}4)$ D-Face of Calcite and the (011) Face of the Alanine Crystal

vector (Å) of the 2D coincidence cell on the $(21\bar{3}4)$ face of calcite	vector (Å) of the 2D coincidence cell on the (011) face of alanine	misfit (%)
$^1/_3[\bar{4}41] = 12.850$	$[0\bar{1}1] = 13.578$	+5.66
$^1/_3[5\bar{2}\bar{2}] = 15.402$	$5 \times [\bar{1}1\bar{1}] = 14.820$	− 3.93
δ = angle between $[\bar{4}41]$ and $[5\bar{2}\bar{2}] = 156.03°$	φ = angle between $[0\bar{1}1]$ and $[\bar{1}1\bar{1}] = 156.37°$	angular misfit −0.33°
area of the 2D coincidence cell 80.387 Å^2	area of the 2D coincidence cell 80.653 Å^2	−0.33

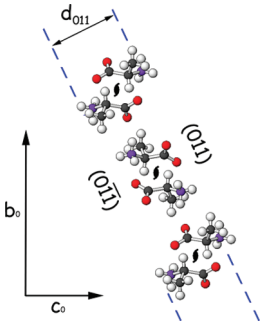

Figure 7. Structure of the L-alanine crystal viewed along the development direction of the PBC [100]. The slice of thickness d_{011} shows that the profiles of the opposite faces (011) and $(0\bar{1}\bar{1})$ are equivalent, owing to the [100] screw dyad axes that lie at the middle of each slice.

the NH_3 and COO, and the same groups in the D configuration outcrop on the (011) and $(0\bar{1}\bar{1})$ faces of the D crystal, respectively. Hence, it is clear that alanine adsorption on the mirror-symmetry-equivalent faces of the scalenohedron had no enantiospecificity.

This further strengthens our hypothesis: *the selectivity belongs neither intrinsically to the crystalline substrate nor to the "size" of the foreign adsorbed molecule, but lies in the compatibility between the substrate and the polar properties of the epitaxially adsorbed 2D layer.*

This way of thinking is also supported by many examples of chiral ordering on crystal surfaces, such as (1) the formation of tartaric acid/succinic acid monolayers on Cu(110) faces,[32] (2) the confinement in 2D layers (in two enantiomeric forms) of PVBA molecules[33] and the supramolecular assembly and chirality in a 2D dicarboxylate network[34] on Cu (100) faces, (3) the chirality introduced, in the 2D oxygen adsorbed phase, by the mechanical stress deforming the oxygen/Cu(110) interface,[35] and (4) the 2D self-assembly of chiral malic acid on Cu(110).[36]

4. CONCLUSIONS

From the Hartman−Perdok analysis carried out on the crystallographic forms of calcite belonging to the $\langle\bar{4}41\rangle$ zone, the following conclusions can be made:

(i) Two forms out of four, the cleavage $\{10\bar{1}4\}$ rhombohedron and the $\{11\bar{2}0\}$secondary prism, show a marked F character, while the flat $\{01\bar{1}8\}$ rhombohedron and the $\{21\bar{3}4\}$ scalenohedron are stepped; this is in open contradiction with the observed occurrence frequency of natural crystals which shows an opposite order, i.e., $\{21\bar{3}4\} > \{01\bar{1}8\} > \{10\bar{1}4\} > \{11\bar{2}0\}$. Moreover, the Bravais−Friedel−Donnay−Harker geometrical law on the morphological importance of the crystallographic forms is also violated since, according to BFDH, one should obtain $\{10\bar{1}4\} > \{11\bar{2}0\} > \{01\bar{1}8\} > \{21\bar{3}4\}$.

(ii) The values of the athermal energies of the surfaces generated by the HP analysis (PBC method) indicate that, within the $[\bar{4}41]$ zone, only the cleavage $\{10\bar{1}4\}$ rhombohedron can belong to the theoretical ES of the calcite crystal, so confirming our previous findings.[28] Nevertheless, a minor reduction of the surface energy values of both $\{01\bar{1}8\}$ and $\{21\bar{3}4\}$ forms, obtainable when calculating the surface energy at room temperature, could be sufficient to make the ES richer with these stepped forms. This result is not negligible since an ES formed by the $\{10\bar{1}4\}$, $\{01\bar{1}2\}$, $\{10\bar{1}0\}$, and {0001} forms, plus the just mentioned $\{01\bar{1}8\}$ and $\{21\bar{3}4\}$ forms, represents the best prerequisite to explain the extraordinary richness of the growth morphology of calcite, even if water adsorption is not considered.

Considering surface relaxation was confirmed to be a necessary condition to obtain a *realistic representation of the surface energy anisotropy*. As a matter of fact, relaxation lowers by about 24% the surface energy of the most compact and flat $\{10\bar{1}4\}$ form, while the corresponding values of the stepped and relaxed $\{01\bar{1}8\}$ and $\{21\bar{3}4\}$ forms are reduced by about 44% and 46%, respectively.

In this paper, we carefully focused our analysis on the $\{21\bar{3}4\}$ scalenohedron and examined, for the first time, its surface profile to better understand the complexity of the adsorption phenomena occurring at the interface between the so-called "chiral faces" of calcite and the enantiomers of some amino acids. Being inspired by our preceding findings on the influence of the 2D epitaxial layers acting as habit modifiers, we searched for epitaxies: (i) between the D and L $\{21\bar{3}4\}$ surfaces and the adsorbed 2D layers of polar {010} and $\{0\bar{1}0\}$ L-Asp; (ii) between the $\{10\bar{1}4\}$ surface and the adsorbed 2D Asp layers; (iii) between the D and L $\{21\bar{3}4\}$ surfaces and the adsorbed 2D layers of the {011} form of alanine crystal.

For the time being, our work was limited to assess the importance of the 1D and 2D epitaxies as sources of the enantiospecificity. In other words, we attempted to show that the stronger adsorption obtains when 2D lattice coincidences occur at the host/guest interface. In this case, i.e., when also the interactions among the adsorbed molecules is taken into account, the most realistic adhesion energy value (per molecule) is represented by the average over the number of molecules belonging to the 2D coincidence cell: the smaller its multiplicity, the higher the probability that a 2D epitaxy can occur on terraces, either between spreading steps or at crystal−solution equilibrium. The same reasoning applies when a 1D epitaxy obtains between a step edge and a molecular adsorbed row.

These are the main reasons why we chose the "cooperative molecular" approach, instead of searching for the best interaction of a "single adsorbed molecule on specific surface sites".

AUTHOR INFORMATION

Corresponding Author

*E-mail: dino.aquilano@unito.it. Phone: +390116705125. Fax: +390116705128.

■ ACKNOWLEDGMENT

We express special thanks to the reviewers for both criticism and gratifying appreciation. We are also grateful to Mrs. Jeanne Griffin for improving the readability of the text.

■ REFERENCES

(1) Statistical data obtained from consulting: (a) Goldschmidt, V. *Atlas der Kristallformen*; Carl Winters Universität-Verlag: Heidelberg, Germany, 1923−1931; Vols. 1−9. (b) Sunagawa, I. *Geol. Surv. Jpn. Rep.* **1953**, *155*, 1–66.

(2) Hartman, P. In *Crystal Growth: An Introduction*, Hartman, P., Ed.; North-Holland Publishing Co.: Amsterdam, 1973; pp 367−402.

(3) Massaro, F. R.; Bruno, M.; Aquilano, D. *Cryst. Growth Des.* **2010**, *10*, 4096–4100.

(4) Aquilano, D.; Calleri, M.; Natoli, E.; Rubbo, M.; Sgualdino, G. *Mater. Chem. Phys.* **2000**, *66*, 159–163.

(5) Hazen, R. M.; Filley, T. R.; Goodfriend, G. A. *Proc. Natl. Acad. Sci. U.S.A.* **2001**, *98*, 5487–5490.

(6) Hazen, R. M.; Brandes, J. A.; Yoder., H. S. J. *Trans. Am. Geophys. Union* (Abstract) **2002**.

(7) Downs, R. T.; Hazen, R. M. *J. Mol. Catal. A* **2004**, *216*, 273–286.

(8) Hazen, R. M. In *Progress in Biological Chirality*; Palyi, G., Zucchi, C., Caglioti, L., Eds.; Elsevier: Oxford, U.K., 2004; pp 137−151.

(9) Hazen, R. M. *Am. Mineral.* **2006**, *91*, 1715–1729.

(10) Asthagiri, A.; Hazen, R. M. *Mol. Simul.* **2007**, *33* (4−5), 343–351.

(11) Pastero, L.; Aquilano, D.; Costa, E.; Rubbo, M. *J. Cryst. Growth* **2005**, *275*, e1625–e1630.

(12) Wenk, H. R. ; Barber, D. J. ; Reeder R. J. In *Carbonates: Mineralogy and Chemistry*; Reeder, R. J., Ed.; Reviews in Mineralogy, Vol. 11; Mineralogical Society of America: Chantilly, VA, 1990; pp 301−367.

(13) Rohl, A. L.; Wright, K.; Gale, J. D. *Am. Mineral.* **2003**, *88*, 921–925.

(14) Gale, J. D. *J. Chem. Soc., Faraday Trans.* **1997**, *93*, 629–637.

(15) Dovesi, R.; Civalleri, B.; Orlando, R.; Roetti, C.; Saunders, V. R. In *Ab Initio Quantum Simulation in Solid State Chemistry*; Lipkowitz, B. K., Larter, R., Cundari, T. R., Eds.; Reviews in Computational Chemistry, Vol. 21; John Wiley and Sons Inc.: New York, 2005; pp 1−125.

(16) Friedel, G. *Bull. Soc. Fr. Mineral.* **1907**, *30*, 326–455.

(17) Donnay, J. D. H.; Harker, D. *Am. Mineral.* **1937**, *22*, 446–467.

(18) Pastero, L.; Costa, E.; Bruno, M.; Rubbo, M.; Sgualdino, G.; Aquilano, D. *Cryst. Growth Des.* **2004**, *4* (3), 485–490.

(19) Massaro, F. R.; Pastero, L.; Costa, E.; Sgualdino, G.; Aquilano, D. *Cryst. Growth Des.* **2008**, *8* (6), 2041–2046.

(20) Pastero, L.; Aquilano, D. *Cryst. Growth Des.* **2008**, *8* (9), 3451–3460.

(21) Bittarello, E.; Massaro, F. R.; Rubbo, M.; Aquilano, D. *Cryst. Growth Des.* **2009**, *9* (2), 971–977.

(22) Bittarello, E.; Massaro, F. R.; Aquilano, D. *J. Cryst. Growth* **2010**, *312*, 402–412.

(23) Derissen, J. L.; Endeman, H. J.; Peerdeman, A. F. *Acta Crystallogr., B* **1968**, *24*, 1349–1354.

(24) Kern, R.; Métois, J. J.; Le Lay, G. In *Basic Mechanisms in the Early Stages of Epitaxy*; Kaldis, E., Ed.; Current Topics in Materials Science, Vol. 3, North-Holland Publishing Co.: Amsterdam, 1979; pp 131−419.

(25) Sumner, D. W. *Am. J. Sci.* **1997**, *297*, 455–487.

(26) Lowenstam, H. A.; Weiner, S. *On Biomineralization*; Oxford University Press: New York, 1989.

(27) Paquette, J.; Reeder, R. J. *Geochim. Cosmochim. Acta* **1995**, *59*, 735–749.

(28) Teng, H. H.; Dove, P. M.; Orme, C. A.; De Yoreo, J. J. *Science* **1998**, *282*, 724–727.

(29) Bruno, M.; Massaro, F. R.; Prencipe, M.; Aquilano, D. *CrystEngComm* **2010**, *12*, 3626–3633.

(30) Kristensen, R.; Stipp, S. L. S.; Refson, K. *J. Chem. Phys.* **2004**, *121*, 8511–8523.

(31) Wilson, C. *New J. Chem.* **2005**, *29*, 1318–1322.

(32) Parschau, M.; Romer, S.; Ernst, K. H. *J. Am. Chem. Soc.* **2004**, *126*, 15398–15399.

(33) Vidal, F.; Delvigne, E.; Stepanow, S.; Lin, N.; Barth, J. V.; Kern, K. *J. Am. Chem. Soc.* **2005**, *127*, 10101–10106.

(34) Stepanow, S.; Lin, N.; Vidal, F.; Landa, A.; Ruben, M.; Barth, J. V.; Kern, K. *Nano Lett.* **2005**, *5*, 901–904.

(35) Guillemot, L.; Bobrov, K. *Phys. Rev. B* **2009**, *79*, 201406 (R.

(36) Roth, C.; Passerone, D.; Merz, L.; Parschau, M.; Ernst, K. H. *J. Chem. Phys. C* **2011**, *115*, 1240–1247.